Soft Multi-organ Shape Models via Generalized PCA: A General Framework

Juan J. Cerrolaza[1(✉)], Ronald M. Summers[2], and Marius George Linguraru[1,3]

[1] Sheikh Zayed Institute for Pediatric Surgical Innovation, Children's National Health System, Washington, D.C., USA
{JCerrola,MLingura}@cnmc.org
[2] Department of Radiology and Imaging Sciences, National Institute of Health, Bethesda, MD, USA
[3] School of Medicine and Health Sciences, George Washington University, Washington, D.C., USA

Abstract. This paper addresses the efficient statistical modeling of multi-organ structures, one of the most challenging scenarios in the medical imaging field due to the frequently limited availability of data. Unlike typical approaches where organs are considered either as single objects or as part of predefined groups, we introduce a more general and natural approach in which all the organs are inter-related inspired by the rhizome theory. Combining canonical correlation analysis with a generalized version of principal component analysis, we propose a new general and flexible framework for multi-organ shape modeling to efficiently characterize the individual organ variability and the relationships between different organs. This new framework called SOMOS can be easily parameterized to mimic a wide variety of alternative statistical shape modeling approaches, including the classic point distribution model, and its more recent multi-resolution variants. The significant superiority of SOMOS over alternative approaches was successfully verified for two different multi-organ databases: six subcortical structures of the brain, and seven abdominal organs. Finally, the organ-prediction capability of the model also significantly outperformed a partial least squared regression-based approach.

Keywords: Shape models · Generalized PCA · Multi-organ · Hierarchical model

1 Introduction

Organ modeling and shape analysis are of crucial importance in the development of robust diagnostic tools, treatment planning, and patient follow-up. However, most statistical shape models have focused on single organ-based applications, proven inefficient when dealing with the variability of the shape and position of some challenging anatomical structures (e.g. the pancreas). Shifting from organ-based to organism-based approaches, there has been growing interest in the development of comprehensive and holistic computational anatomical models in recent years [1–3]. However, as the complexity and detail of anatomical models increase, there are new

S. Ourselin et al. (Eds.): MICCAI 2016, Part III, LNCS 9902, pp. 219–228, 2016.
DOI: 10.1007/978-3-319-46726-9_26

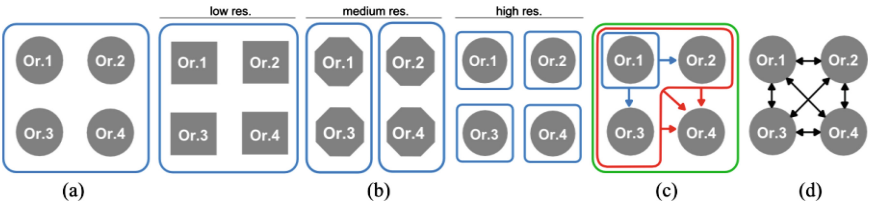

Fig. 1. Multi-organ shape modeling strategies. (a) Classic PDM: all the organs (Or.) are modeled together as a single object. (b) Multi-resolution hierarchical model [1]: all the organs are modeled together at coarser resolutions, modeling smaller groups as we move toward finer resolutions. In the picture, square, octagons, and circles, represent low, intermediate, and high resolution of the organs, respectively. (c) Sequential organ modeling [2]: Or.1 is used to estimate Or.2 and Or.3. Or.1, Or.2, and Or.3 will be used to estimate Or.4. (d) Rhizomatic structure: all the inter-organ relationships are considered in the model.

technical challenges that hinder the use of traditional shape modeling methods, such as the limited availability of data. While a limited number of examples may be sufficient to model relatively simple organs, such as the kidneys, an adequately large training set is not always available as the dimensionality and complexity of the structures increase. This issue is known as the high-dimension-low-sample-size (HDLSS) problem.

One of the most popular shape modeling techniques is the Point Distribution Model (PDM) proposed by Cootes et al. [4]. Despite the inherent capability of PDMs to model multi-organ structures by performing global statistics on all the objects (see Fig. 1(a)), these models are particularly sensitive to the HDLSS issue. Moreover, PDMs do not represent object-based scale level, which limits their ability to describe the local geometry information of organs. More recently, Cerrolaza et al. [1] proposed a new generalized multi-resolution hierarchical variant of PDM (GEM-PDM). Based on a multi-resolution decomposition of the shapes, GEM-PDM defines clusters of organs that are modeled together at each resolution (see Fig. 1(b)), providing an efficient characterization of the inter-organs relations, as well as the particular locality of each organ. Although GEM-PDM is robust for general multi-organ modeling, the hierarchical configuration may be affected by some design parameters of the model. The inter-organ relations were also explored by Okada et al. [2], presenting an automated framework for the modeling and segmentation of multiple abdominal organs in CT images (Fig. 1(c)). Based on a predefined ranking of organ stability, the authors defined a sequential modeling of the organs designed to improve the analysis of challenging structures, such as the pancreas, using information from neighboring stable organs, such as the liver and spleen.

Unlike the classic rigid organization of the information as a unified structure ruled by hierarchy [1] or linearity [2], the rhizomatic structure developed by Deleuzed and Guattari [5] proposes an alternative organization of the information units (e.g., organs) as an interconnected, non-linear network. Inspired by this new concept, we propose a new general framework for SOft Multi-Organ Shape models (SOMOS). In SOMOS, a multi-organ structure is modeled by a graph (see Fig. 1(d)), whose nodes and edges represent the organs and the relationships between them, respectively. Based on generalized principal component analysis (G-PCA), the flexibility of the SOMOS also

allows to replicate previous approaches (e.g. PDM, GEM-PDM) by defining particular parameterizations of the model (i.e., imposing hard inter-organ constraints). However, the rhizomatic nature of SOMOS assumes the general scenario where all the inter-organ relationships are considered in the model, bringing together the advantages of all those alternative approaches in a common flexible framework.

2 Shape Models

Let $\{\boldsymbol{x}_1, \ldots, \boldsymbol{x}_M\}$ be the set of $M \in \mathbb{N}$ organs in a d-dimensional ($d = 2$ or 3) space. Each $\boldsymbol{x}_j$ $(1 \leq j \leq M)$ represents the vector form of a single-object structure defined by the concatenation of the $K_j \in \mathbb{N}$ landmarks that define each organ (i.e., $\boldsymbol{x}_j = (x_{j(1)}, \ldots, x_{j(d \cdot K_j)})^T$). In the same way, $\boldsymbol{x}$ is defined as the $(d \cdot K \times 1)$ vector resulting from the concatenation of the M organs, $\boldsymbol{x} = (\boldsymbol{x}_1; \ldots; \boldsymbol{x}_M)^{\boldsymbol{T}}$, and $K = \sum K_j$. Unlike the classic PDM, where a single global shape model is built for $\boldsymbol{x}$, SOMOS creates M individual models, one for each organ of interest. The goal of each individual model is, not only to characterize the particular anatomical variability of a particular organ (i.e. a node in the graph), but also its relationships with any other structure in the model. The creation of these individual shape models is detailed below.

2.1 Organ-Based Shape Models via Generalized PCA

Consider the creation of the statistical model for the i-th organ, $\boldsymbol{x}_i$. The relationship between $\boldsymbol{x}_i$ and the remaining organs is defined by means of the $(M \times 1)$ vector, $\boldsymbol{w}_i$, whose j-th component, $w_{ij} \in [0, 1]$, represents the correlation between $\boldsymbol{x}_i$ and $\boldsymbol{x}_j$. A factor of 1 means perfect correlation (e.g. $w_{ii} = 1$), while 0 represents the absence of relationship between both organs. An efficient statistical model should be able to model the variability of the organ of interest, $\boldsymbol{x}_i$, as well as those significant inter-organ relationships (i.e. with high values of w_{ij}). Based on the G-PCA formulation proposed by Greenancre [6] we formulate the problem as a weighted variant of PCA.

Let $\boldsymbol{X}$ represents the $(N \times d \cdot K)$ centered data matrix (i.e. zero mean) containing the vector form of the $N \in \mathbb{N}$ training cases. Using the generalized singular value decomposition (G-SVD) [6] of $\boldsymbol{X}$, this matrix can be de written as $\boldsymbol{X} = \boldsymbol{VDB}^T$, where $\boldsymbol{V}$ and $\boldsymbol{B}$ are $(N \times r)$ and $(d \cdot K \times r)$ matrices respectively (r is the rank of $\boldsymbol{X}$), and $\boldsymbol{D}$ is a $(r \times r)$ diagonal matrix. However, unlike classic SVD, $\boldsymbol{V}$ and $\boldsymbol{B}$ are not necessarily orthonormal. In G-SVD, $\boldsymbol{V}$ and $\boldsymbol{B}$ satisfy $\boldsymbol{V}^T\boldsymbol{\Phi}\boldsymbol{V} = \boldsymbol{I}_r$, and $\boldsymbol{B}^T\boldsymbol{\Omega}\boldsymbol{B} = \boldsymbol{I}_r$, with $\boldsymbol{\Phi}$ and $\boldsymbol{\Omega}$ being specified positive-definite symmetric matrices, and $\boldsymbol{I}_r$ the identity matrix of order r. G-SVD finds the ordinary SVD of $\tilde{\boldsymbol{X}} = \boldsymbol{\Phi}^{1/2}\boldsymbol{X}\boldsymbol{\Omega}^{1/2}$. In the particular case in which $\boldsymbol{\Phi}$ and $\boldsymbol{\Omega}$ are diagonal, $\tilde{\boldsymbol{X}}$ can be considered as a weighted version of $\boldsymbol{X}$, where different observations and variables can have different weights. Assuming all the observations are treated identically, we can define $\phi_{11} = \ldots = \phi_{NN} = 1$. SVD of $\tilde{\boldsymbol{X}}$ can be written as $\tilde{\boldsymbol{X}} = \boldsymbol{UEC}^T$, where $\boldsymbol{E}$ is a diagonal matrix and $\boldsymbol{U}^T\boldsymbol{U} = \boldsymbol{C}^T\boldsymbol{C} = \boldsymbol{I}_r$. Then, $\boldsymbol{X} = \tilde{\boldsymbol{X}}\boldsymbol{\Omega}^{-1/2} = \boldsymbol{UEC}^T\boldsymbol{\Omega}^{-1/2}$, and thus $\boldsymbol{V} = \boldsymbol{U}$, $\boldsymbol{D} = \boldsymbol{E}$, and $\boldsymbol{B} = \boldsymbol{\Omega}^{-1/2}\boldsymbol{C}$.

G-PCA is defined by $\boldsymbol{P}$, the $(d \cdot K \times m)$ matrix formed by the first $m \leq$ r columns of $\boldsymbol{B}$. Like in the classic PCA-based PDM [4], each shape can be now modeled as $\boldsymbol{x} \approx \tilde{\boldsymbol{x}} = \bar{\boldsymbol{x}} + \boldsymbol{P} \cdot \boldsymbol{b}$, where $\boldsymbol{b}$ is the $(m \times 1)$ coordinate vector of $\boldsymbol{x}$ in the space defined by $\boldsymbol{P}$. It can be demonstrated that among all possible rank m approximations, $\tilde{\boldsymbol{x}}$ minimizes $\sum_{k=1}^{K} \omega_k \left(\tilde{\boldsymbol{x}}_{(k)} - \boldsymbol{x}_{(k)}\right)^2$. That is, the shape model provides a weighted least square approximation where the contribution of each variable is weighted by $\omega_k \in \mathbb{R}^+$, the diagonal components of $\boldsymbol{\Omega}$. In SOMOS, $\boldsymbol{\Omega}$ is defined by $\boldsymbol{w}_i$ as follow: $\omega_k = w_{ij}$ s.t. $\boldsymbol{x}_{(k)} \in \boldsymbol{x}_j$. Therefore, the resulting shape model for organ $\boldsymbol{x}_i$ not only prioritizes the variability of that organ (which reduces the HDLSS effect in $\boldsymbol{x}_i$), but also considers the context of the organ thanks to its inherent rhizomatic structure.

To define w_{ij}, the correlation factor between two organs, $\boldsymbol{x}_i$ and $\boldsymbol{x}_j$, we use canonical correlation analysis (CCA) between these two sets of variables. CCA determines the linear combinations of the components in $\boldsymbol{x}_i$ that are maximally correlated with linear combinations of the components in $\boldsymbol{x}_j$. The strength of these correlations is described by the corresponding correlation coefficients with values between 0 and 1 (see Fig. 2). The capacity of CCA was previously studied by Rao et al. [7] and Okada et al. [2] to define inter-organ relationships of sub-cortical brain structures. In SOMOS, the overall inter-organ correlation factor, w_{ij}, is defined automatically as the average correlation coefficient over all calculated canonical modes of CCA($\boldsymbol{x}_i$, $\boldsymbol{x}_j$).

2.2 Shape Modeling Using SOMOS

Let $\boldsymbol{y} = (\boldsymbol{y}_1; \ldots; \boldsymbol{y}_M)^T$ be the vector form of any d-dimensional multi-organ structure we want to model using the new SOMOS framework, i.e. finding $\tilde{\boldsymbol{y}} = (\tilde{\boldsymbol{y}}_1; \ldots; \tilde{\boldsymbol{y}}_M)^T$, the best approximation of $\boldsymbol{y}$ in the subspace of valid shapes defined by the set of M statistical models created in Sect. 2.1. For each of these models, $\boldsymbol{y}$ can be approximated as $\left(\tilde{\boldsymbol{y}}_j; \ldots; \tilde{\boldsymbol{y}}_{jM}\right)^T = \bar{\boldsymbol{x}} + \boldsymbol{P}_j \cdot \boldsymbol{b}_j$, where the vector of coefficients $\boldsymbol{b}_j$ is obtained as $\boldsymbol{b}_j = \mathbf{P}_j^T \boldsymbol{\Omega}_j^{1/2} (\boldsymbol{y} - \bar{\boldsymbol{x}})$. Thus, the j-th organ in $\tilde{\boldsymbol{y}}$, $\tilde{\boldsymbol{y}}_j$, is modeled by $\tilde{\boldsymbol{y}}_{jj}$.

3 SOMOS: General Framework for Shape Modeling

SOMOS can be considered as a generalization of the traditional shape models able to integrate alternative methods in a common framework. In the particular case in which $\boldsymbol{\Omega} = \mathbf{I}$ (i.e., $\boldsymbol{w}_{ij} = 1$, $\forall i,j$) SOMOS becomes equivalent to the original PDM [4] (and thus, suffering from HDLSS). On the other hand, defining $w_{ij} = \delta_{ij}$, where δ_{ij} is the Kronecker delta function, the model becomes equivalent to an independent modeling of each organ (and thus, not integrating into the model relevant inter-organ relationships). Other interesting applications of the SOMOS framework are presented below.

3.1 Multi-resolution Hierarchical Multi-organ Shape Modeling

Suppose now $\{\boldsymbol{x}^r\}_{r=0,\ldots,R}$ represents the multi-resolution (MR) decomposition of the shape $\boldsymbol{x}$, where $\boldsymbol{x}^0$ and $\boldsymbol{x}^R$ represent the finest and the coarsest level of resolution, respectively. The detail information missed from $\boldsymbol{x}^r$ to $\boldsymbol{x}^{r-1}$ is represented by the corresponding high-frequency vector $\boldsymbol{z}^r$. From $\boldsymbol{x}^0$, $\{\boldsymbol{x}^r\}_{r=0,\ldots,R}$ and $\{\boldsymbol{z}^r\}_{r=1,\ldots,R}$ can be obtained using the corresponding analysis equations: $\boldsymbol{x}^r = \boldsymbol{A}^r\boldsymbol{x}^{r-1}$, and $\boldsymbol{z}^r = \boldsymbol{H}^r\boldsymbol{x}^{r-1}$, respectively, where $\boldsymbol{A}$ and $\boldsymbol{H}$ are the analysis filters (see [8] for details). Similarly to the work proposed by Cerrolaza et al. [1], SOMOS can incorporate MR shape analysis as follows. Imposing the initial condition that $\boldsymbol{\Omega}^R = \mathbf{I}$ (i.e. a global model of the entire multi-organ structure is built at the coarsest resolution to guarantee the coherent disposition of the elements), G-PCA is used at each level of resolution obtaining $\left\{\bar{\boldsymbol{x}}^r, \boldsymbol{P}_j^r, \boldsymbol{\Omega}_j^r\right\}_{j=1,\ldots,M;r=0,\ldots R}$. However, unlike the original framework proposed in [1] where a hard separation of organs was required at each resolution (i.e., $\boldsymbol{w}_{ij}^r = 0$ or 1) (see Fig. 1(b)), we propose the use of new inter-organ correlation factors defined as $\hat{\Omega}_j^r = \prod_{k=r}^{R} \boldsymbol{\Omega}_j^k$, where $\boldsymbol{\Omega}_j^k$ are the correlation factors at resolution k obtained via CCA, as described in Sect. 2.1. Since $\boldsymbol{w}_{ij}^r \in (0,1)$, the inter-organ information incorporated by the model, $\hat{\Omega}_j^r$, decreases as we move towards finer level or resolution, and thus, reducing the HDLSS effect. Starting from the finest resolution, the fitting of a new shape $\boldsymbol{y}$ is obtained by applying the modeling process described in Sect. 2.2 at each resolution, $\{\boldsymbol{y}^r\}_{r=0,\ldots,R}$. The high frequency component of the new constrained shape $\tilde{\boldsymbol{y}}^r$, $\tilde{\boldsymbol{z}}^r$, is used to recover the original resolution at the end of the process using the corresponding synthesis filters: $\tilde{\boldsymbol{y}}^{r-1} = \boldsymbol{F}^r\tilde{\boldsymbol{y}}^r + \boldsymbol{G}^r\tilde{\boldsymbol{z}}^r$ (see [8]).

3.2 Sequential Multi-organ Shape Modeling

Suppose now $\{\boldsymbol{x}_1, \boldsymbol{x}_2, \boldsymbol{x}_3, \boldsymbol{x}_4\}$ represents an ordered sequence of organs from highest to lowest stability, as the one depicted in Fig. 1(c) and presented by Okada et al. [2] for the segmentation of abdominal organs (in this example $\boldsymbol{x}_1$: liver, $\boldsymbol{x}_2$: spleen, $\boldsymbol{x}_3$: left kidney and $\boldsymbol{x}_4$: pancreas; the extension to a more general scenario with K organs is straighforward). In their original work, Okada et al. used partial least square regression (PLSR) to obtain an initial estimation of the organs using the previous ones (i.e., the more stable organs) as predictors (see Fig. 1(c)). This initial segmentation was further refined via probability atlas and a shape model of the residuals. This sequential modeling of organs can be easily modeled in SOMOS as follows. Starting with the most stable organ, $\boldsymbol{x}_1$, the elements of $\boldsymbol{\Omega}_1$ are defined as $w_{ij} = \delta_{1j}$, thereby preventing the propagation of errors from less table organs. Having modeled $\boldsymbol{x}_1$, $\boldsymbol{\Omega}_2$ and $\boldsymbol{\Omega}_3$ are defined as $w_{ij} = \delta_{\{1,2\}j}$ and $w_{ij} = \delta_{\{1,3\}j}$, respectively, where $\delta_{\{i,k\}j} = 1$ if $j \in \{i,k\}$, and 0 otherwise. Similarly, $\boldsymbol{\Omega}_4$ is defined as $w_{ij} = \delta_{\{1,2,3\}j}$, i.e. all the previous organs will be used to model the least stable organ, the pancreas. When modeling the less stable structures in a new shape $\boldsymbol{y} = (\boldsymbol{y}_1; \boldsymbol{y}_2; \boldsymbol{y}_3; \boldsymbol{y}_4)^T$, the influence of these organs estimating $\boldsymbol{b}_j$ can be controlled by means of the classic weighted PDM formulation [9]

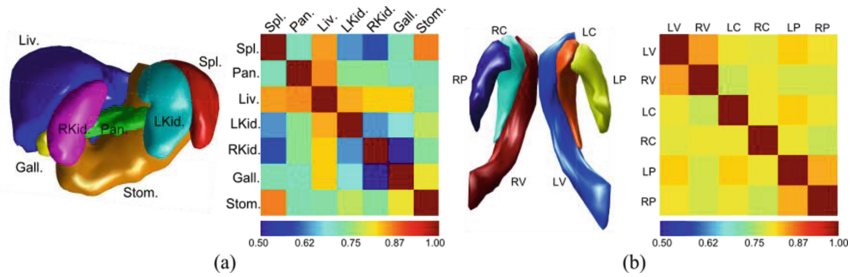

Fig. 2. Canonical Correlation Analysis (CCA) of the organs. (a) CCA of 7 abdominal organs: Spleen (Spl.), pancreas (Pan.), liver (Liv.), left kidney (LKid), right kidney (RKid), gallblader (Gall.) and stomach (Stom.). (b) CCA of 6 subcortical structures: left and right lateral ventricles (LV, RV), left and right caudate nuclei (LC, RC), and left and right putamens (LP,RP).

$\boldsymbol{b_j} = \left(\mathbf{P}_j^T \boldsymbol{\Psi}_j \mathbf{P}_j\right)^{-1} \mathbf{P}_j^T \boldsymbol{\Omega}_j^{1/2} (\boldsymbol{y} - \bar{\boldsymbol{x}})$. In particular, $\boldsymbol{\Psi}_j$ is a $(d \cdot K \times d \cdot K)$ diagonal matrix with corresponding weight value (i.e., reliability) for each landmark. Thus, $diag(\boldsymbol{\Psi}_1) = (1_{K_1}, 0_{K_2}, 0_{K_3}, 0_{K_4})$, $diag(\boldsymbol{\Psi}_2) = (1_{K_1}, \psi_2 \cdot 1_{K_2}, 0_{K_3}, 0_{K_4})$, $diag(\boldsymbol{\Psi}_3) = (1_{K_1}, 0_{K_2}, \psi_3 \cdot 1_{K_3}, 0_{K_4})$, and $diag(\boldsymbol{\Psi}_2) = (1_{K_1}, \psi_2, 1_{K_2}, \psi_3 \cdot 1_{K_3}, \psi_4, 1_{K_4})$, where 1_k and 0_k represent $(1 \times d \cdot K)$ vectors of 1's and 0's respectively, and $\psi_j \in [0, 1]$ are constants indicating the stability of each organ (and thus, $1 = \psi_1 > \psi_2 \geq \psi_3 > \psi_4$). Similarly to the method proposed by Okada et al. [2], this SOMOS-based sequential shape model can turn into a predictive model for the particular case in which $\psi_2 = \psi_3 = \psi_4 = 0$ (i.e., $\boldsymbol{x}_2$, $\boldsymbol{x}_3$, and $\boldsymbol{x}_4$ are estimated by $\boldsymbol{x}_1$).

4 Results and Discussion

We use two different datasets to evaluate the ability of SOMOS to model multi-organ structures: a database of 18 CT abdominal studies (voxel resolution: 0.58 × 0.58 1.00 mm; volume: 512 × 512 × 360) including seven organs (see Fig. 2(a)), and a public database of 18 T1-weighted brain MRI volumes [10] (voxel resolution: 0.94 × 0.94 × 1.50 mm; volume: 256 × 256 × 256 with six subcortical structures (see Fig. 2 (b)).

The most general multi-resolution version of SOMOS (MR-SOMOS) described in Sect. 3.1 is compared with two alternative approaches: GEM-PDM [1], and PDM [4]. Thanks to the flexibility of SOMOS, both approaches, PDM and GEM-PDM, were implemented using the same common framework, to which we refer to as SOMOS-PDM and SOMOS-GEM, respectively. Thus, we define R = 0 and $\boldsymbol{\Omega}^0 = \boldsymbol{I}$ to generate SOMOS-PDM. In SOMOS-GEM we define hard separations between groups of organs at each level of resolution (i.e., $\boldsymbol{w}_{ij}^r = 0$ or 1), following the configuration detailed in [1]. The number of resolution levels is set to 5 (i.e., R = 4) for both, MR-SOMOS and SOMOS-GEM. To characterize the accuracy of the three methods to model new instances we compute the symmetric landmark-to-surface distance (L2S) and Dice coefficient (DC), using leave-one-out cross-validation.

Table 1. Abdominal database – shape modeling accuracy of 7 abdominal structures; * marks statistically significant improvement over PDM; ● marks statistically significant improvement over PDM and GEM (p-value < 0.01).

DC	Spl.	Pan.	Liv.	LKid.	RKid.	Gall.	Stom.	Avg.
MR-SOMOS	●0.85±0.05	*0.82±0.08	*0.86±0.03	●0.87±0.03	*0.87±0.04	●0.74±0.11	*0.83±0.03	●0.82±0.08
SOMOS-GEM	0.82±0.08	0.83±0.05	0.86±0.03	0.74±0.09	0.87±0.04	0.69±0.10	0.82±0.04	0.80±0.09
SOMOS-PDM	0.77±0.08	0.78±0.07	0.82±0.04	0.73±0.14	0.76±0.07	0.60±0.13	0.74±0.06	0.73±0.12
L2S(mm)	Spl.	Pan.	Liv.	LKid.	RKid.	Gall.	Stom.	Avg.
SOMOS	●2.76±0.88	*2.78±0.94	*4.74±1.05	●2.43±0.70	*2.53±0.70	*2.71±1.00	*3.75±1.10	*3.10±1.20
SOMOS-GEM	4.41±0.66	2.74±0.88	3.20±1.30	3.49±1.18	4.05±1.14	3.18±0.99	2.36±0.80	3.35±1.19
SOMOS-PDM	5.60±1.07	3.90±1.33	4.68±1.47	4.57±1.65	5.96±1.81	4.18±1.50	4.50±1.30	4.77±1.59

The results obtained for the abdominal database are shown in Table 1. The new MR-SOMOS (avg. DC: 0.82 ± 0.08; avg. L2S: 3.10 ± 1.20 mm) provides statistically significant improvement (Wilcoxon signed rank test with p-value < 0.01) over both, SOMOS-GEM (avg. DC: 0.80 ± 0.09; avg. L2S: 3.35 ± 1.19 mm) and SOMOS-PDM (avg. DC: 0.73 ± 0.12; avg. L2S: 4.77 ± 1.59 mm). The superiority of the new framework is also proven in the brain database (Table 2). The average DC are 0.93 ± 0.05, 0.87 ± 0.04 and 0.85 ± 0.05, and the average L2S are 0.61 ± 0.13, 0.68 ± 0.11 and 0.78 ± 0.25 mm, for MR-SOMOS, SOMOS-PDM, and SOMOS-GEM, respectively.

Next, we also evaluate the predictive capability of the new framework to estimate a sequence of organs. In particular, we use the four-organ sequence proposed by Okada et al. [2]. Starting with an initial model of the liver, the authors of [2] estimated the spleen and the left kidney via PLSR. The pancreas was finally estimated using the previous three organs as predictors. This PLSR-based approach is compared with the SOMOS predictive model (Sect. 3.2); results are shown in Table 3. The shape of the liver obtained in the previous experiment is used in both cases. It can be observed how the G-PCA-based estimation provided by SOMOS significantly outperforms PLSR-based models ($p < 0.01$) in terms of DC and L2S metric for all the analyzed organs. The ultimate goal is not to provide a final shape, but to generate a shape model-based initial estimation of challenging organs, such as the pancreas, from more stable organs, that will be refined later by other methods (e.g., probabilistic atlas or texture models). Therefore, the metrics shown in Table 1 are better than those shown in Table 3, where only the liver is used to estimate the spleen, left kidney, and spleen.

The computational cost of SOMOS (∼ 2 min.) is slightly higher than alternative approaches (PDM: ∼ 30 s.; GEM: ∼ 1 min.) due to the iterative modeling over each organ (Matlab® R2015a, 64-bits 2.80 GHz Intel® Xeon® with 16 GB or RAM).

Table 2. Brain database – shape modeling accuracy of 6 subcortical structures.

DC	LV	RV	LC	RC	LP	RP	Avg.
SOMOS	*0.86 ±0.06	●0.92 ±0.04	●0.92 ±0.03	●0.93 ±0.01	*0.93 ±0.01	●0.97 ±0.02	●0.93 ±0.05
SOMOS-GEM	0.84 ±0.05	0.84 ±0.04	0.88 ±0.02	0.87 ±0.03	0.90 ±0.01	0.91 ±0.01	0.87 ±0.04
SOMOS-PDM	0.81 ±0.05	0.80 ±0.05	0.87 ±0.03	0.86 ±0.03	0.89 ±0.03	0.98 ±0.02	0.85 ±0.05
L2S(mm)	LV	RV	LC	RC	LP	RP	Avg.
SOMOS	●0.77 ±0.18	●0.76 ±0.20	●0.51 ±0.15	●0.56 ±0.14	●0.55 ±0.08	●0.50 ±0.14	●0.61 ±0.13
SOMOS-GEM	0.82 ±0.19	0.81 ±0.20	0.60 ±0.09	0.68 ±0.14	0.60 ±0.0.09	0.59 ±0.0.06	0.68 ±0.11
SOMOS-PDM	0.99 ±0.21	1.04 ±0.32	0.66 ±0.14	0.70 ±0.14	0.66 ±0.15	0.66 ±0.11	0.78 ±0.25

Table 3. Organ Prediction Model; ● marks statistically significant improvement (p-val. < 0.01).

DC	Liv.	Spl.	LKid.	Pan.
SOMOS	0.87±0.03	●0.66±0.12	●0.79±0.06	●0.51±0.10
PLSR	0.87±0.03	0.43±0.18	0.51±0.12	0.38±0.14

L2S(mm)	Liver	Spleen	L Kidney	Pancreas
SOMOS	2.27±0.68	●5.60±1.62	●3.77±0.92	●5.40±1.64
PLSR	2.27±0.68	12.46±8.20	9.78±3.20	7.77±3.00

5 Conclusions

We presented SOMOS, a new general framework for multi-organ shape modeling. Unlike typical multi-organ approaches where hard divisions between organs are defined, we adopt a more flexible and natural model: a rhizomatic structure in which all the objects are inter-connected. Using CCA to parameterize the model automatically, we propose a new set of weighted statistical shape models able to characterize efficiently the relationships of each organ with the surrounding structures, as well as its own individual variability. Based on a generalization of PCA, the formulation proposed here integrates easily and naturally not only the SOMOS framework, but also previous approaches in the literature, such as the classic PDM, or the most recent GEM-PDM. Experiments with two different databases (abdomen and brain) demonstrate that the new method significantly outperforms alternative approaches in terms of model accuracy, and organ estimation capabilities. Finally, we also evaluated the prediction capability of SOMOS showing a significant improvement over the alternative PLSR-based approach. In the near future we plan to continue expanding the new framework to integrate temporal variability of organs, and non-linear PDM.

Acknowledgment. This project was supported by a philanthropic gift from the Government of Abu Dhabi to Children's National Health System.

References

1. Cerrolaza, J.J., et al.: Automatic multi-resolution shape modeling of multi-organ structures. Med. Image Anal. **25**(1), 11–21 (2015)
2. Okada, T., et al.: Abdominal multi-organ segmentation from ct images using conditional shape-location and unsupervised intensity priors. Med. Image Anal. **26**(1), 1–18 (2015)
3. Wolz, R., et al.: Automated abdominal multi-organ segmentation with subject-specific atlas generation. IEEE Trans. Med. Image **32**(9), 1723–1730 (2013)
4. Cootes, T.F., et al.: Active shape models their training and application. Comput. Vis. Image Underst. **61**(1), 38–59 (1995)
5. Deleuze, G., Guattari, F.: A Thousand Plateaus. Les Editions de Minuit, Paris (1980)
6. Greenacre, M.J.: Theory and Applications of Correspondence Analysis. Academic Press, New York (1984)

7. Rao, A., et al.: Hierarchical statistical shape analysis and prediction of sub-cortical brain structures. Med. Image Anal. **12**(1), 55–68 (2008)
8. Lounsbery, M., et al.: Multiresolution analysis for surfaces of arbitrary topological type. ACM Trans. Graph. **16**(1), 34–73 (1997)
9. Cootes, T.F., Taylor, C.J.: Active shape model search using local grey-level models: a quantitative evaluation. In: BMVC (1993)
10. IBSR. The Internet Brain Segmentation Repository (IBSR). http://www.cma.mgh.harvard.edu/ibsr/